



No Evolution in the Half-mass Radius of Milky Way–type Galaxies over the Last 10 Gyr

Maryam Hasheminia^{1,2,3} , Moein Mosleh^{1,2} , Sandro Tacchella^{4,5} , S. Zahra Hosseini-ShahiSavandi¹ , Minjung Park⁶ , and Rohan P. Naidu⁶

¹ Biruni Observatory, School of Science, Shiraz University, Shiraz 71946-84795, Iran; moein.mosleh@shirazu.ac.ir

² Department of Physics, School of Science, Shiraz University, Shiraz 71946-84795, Iran

³ Department of Physics, Institute for Advanced Studies in Basic Sciences (IASBS), P.O. Box 11365-9161, Zanjan, Iran

⁴ Kavli Institute for Cosmology, University of Cambridge, Madingley Road, Cambridge, CB3 0HA, UK

⁵ Cavendish Laboratory, University of Cambridge, 19 JJ Thomson Avenue, Cambridge, CB3 0HE, UK

⁶ Center for Astrophysics | Harvard & Smithsonian, 60 Garden Street, Cambridge, MA 02138, USA

Received 2022 April 13; revised 2022 June 1; accepted 2022 June 3; published 2022 June 17

Abstract

The Milky Way (MW) galaxy is in focus, thanks to new observational data. Here we shed new light on the MW's past by studying the structural evolution of MW progenitors, which we identify from extragalactic surveys. Specifically, we constrain the stellar-mass growth history (SMGH) of the MW with two methods: (i) direct measurement of the MW's star formation history, and (ii) assuming the MW is a typical star-forming galaxy that remains on the star-forming main sequence. We select MW progenitors based on these two SMGHs at $z = 0.2$ – 2.0 from the CANDELS/3D-HST data. We estimate the structural parameters (including half-mass radius r_{50} and Sérsic index) from the stellar-mass profiles. Our key finding is that the progenitors of the MW galaxy grow self-similarly on spatially resolved scales with roughly a constant half-mass radius (~ 2 – 3 kpc) over the past 10 Gyr, while their stellar masses increase by about 1 dex, implying little-to-no inside-out growth. We discover that the radius containing 20% of the stellar mass (r_{20}) decreases by 60% between redshifts of $z = 2.0$ and $z = 0.7$, while the central stellar-mass density (Σ_1) increases by a factor of 1.3 dex over the same time and the Sérsic index changes as $n \propto (1 + z)^{-1.41 \pm 0.19}$. This is consistent with an early ($z > 1$) formation of a thick disk, followed by the formation of a bar that led to an increase in the mass in the core. The formation and evolution of the thin disk had only little impact on the overall half-mass size. We also show that the constant-size evolution of the MW progenitors challenges semiempirical approaches and numerical simulations.

Unified Astronomy Thesaurus concepts: Galaxy evolution (594); Galaxy formation (595); Milky Way formation (1053); Milky Way evolution (1052); Galaxy structure (622); Milky Way Galaxy (1054)

1. Introduction

Understanding the assembly history of the Milky Way (MW) galaxy is of great interest because we live within it and because the MW—as a typical disk galaxy—provides a unique probe of galaxy evolution. Thanks to invaluable data from Gaia (Collaboration et al. 2018) and other surveys (e.g., Conroy et al. 2019), recent studies allowed us to put better constraints on the stellar-mass growth history (SMGH) of the MW and produced a picture in which most of the MW stellar mass is assembled in situ over the last 8–11 Gyr (e.g., Belokurov et al. 2018; Helmi et al. 2018; Bonaca et al. 2020; Kruijssen et al. 2020). In this work, we connect these recent insights to extragalactic studies to shed new light on the structural evolution of the MW and disk galaxies in general.

Observationally, it remains challenging to understand how individual galaxies assemble and evolve about scaling relations (e.g., Abramson et al. 2016; Tacchella et al. 2016). In particular, regarding the structural evolution of galaxies, recent observational studies compared the structural parameters of galaxies at a fixed stellar mass over time (e.g., van der Wel et al. 2014; Mowla et al. 2019). However, the evolution of galaxies should be traced by linking progenitors and descendants through cosmic time (e.g., Carollo et al. 2013).

Several different approaches have been used to select progenitors. One such approach is the constant cumulative number density method, which assumes that the galaxies have a fixed comoving number density and rank order at all epochs, thereby ignoring mergers and variations in star formation (van Dokkum et al. 2013). Variations in the SMGH can partially be addressed by abundance matching, which leads to an evolving cumulative number density to compare galaxies across cosmic time (Behroozi et al. 2013; Moster et al. 2013; Papovich et al. 2015; Torrey et al. 2015). In this method, observed galaxies are matched to dark matter halos for which the number density evolution can be tracked through simulations. In a third method, as in situ star formation dominates the mass assembly of star-forming galaxies (SFGs), one can trace the SMGH of SFGs from the observed star formation history (SFH) (Renzini 2009; Leitner & Kravtsov 2011; Patel et al. 2013). Because we focus on the MW for which we have good knowledge of the SMGH over the last ~ 10 Gyr and evidence for mostly in situ star formation (e.g., Kruijssen et al. 2019; Bonaca et al. 2020), we adopt this last method in this work.

Concerning the morphology of galaxies, several recent studies have shown that considering the effect of mass-to-light (M_*/L) gradients and hence analyzing the stellar-mass profiles instead of their light profiles is essential to better constrain the structural evolution of galaxies (Tacchella et al. 2015b; Mosleh et al. 2017, 2020; Suess et al. 2019a, 2019b). Moreover, different size definitions can be used to depict changes in subcomponents of galaxies (Cibinel et al. 2013; Miller et al. 2019). Therefore, in this study, we carefully select MW



Original content from this work may be used under the terms of the [Creative Commons Attribution 4.0 licence](https://creativecommons.org/licenses/by/4.0/). Any further distribution of this work must maintain attribution to the author(s) and the title of the work, journal citation and DOI.

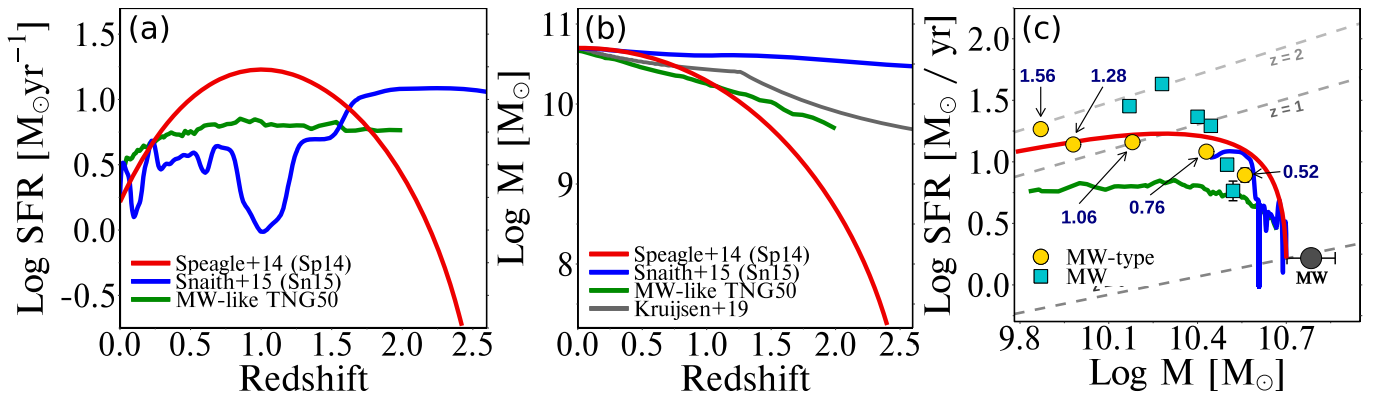


Figure 1. (a) SFH of (i) MW-type galaxies derived by applying the MSI method to the SFR– M_* relation of Sp14 (red line); (ii) the MW from Sn15 (blue line); and (iii) MW-like galaxies in the IllustrisTNG (TNG50) simulation (green line). (b) Corresponding SMGHs with a final stellar mass of $M_{*,0} = 10^{10.7} M_{\odot}$. The SMGH of the MW of Sn15 is in good agreement with Kruijssen et al. (2019), which is shown in gray. (c) Tracks of the MW-type galaxies (red line), the MW (blue line), and the TNG MW-like galaxies (green line) in the SFR– M_* plane. The yellow circles and cyan squares are the median values of the M_* -selected MW-type and MW progenitors at the different redshifts (indicated with the labels). The dashed gray lines indicate the SFR– M_* relation of Sp14. The large gray circle is the M_* and SFR of the MW estimated by Licquia & Newman (2015).

progenitors and use the mass-based structural parameters to revisit the buildup of the MW stellar-mass profile (Section 2). We find negligible evolution in the half-mass size of MW-type galaxies over the past 10 Gyr (Section 3), implying little-to-no inside-out growth of such disk galaxies (Section 4). We show that this is largely independent of the assumed SMGH as the half-mass size versus stellar-mass relation is flat and nearly redshift invariant.

2. Data and Sample Selection

2.1. Observational Data

We aim at selecting star-forming progenitors of MW-type galaxies with a total stellar mass of $\approx 5 \times 10^{10} M_{\odot}$ in the present-day universe (McMillan 2017). We use the CANDELS/3D-HST catalogs (Skilton et al. 2014) to identify those progenitors at earlier cosmic times. We cross-matched this sample with the Mosleh et al. (2020) catalog, which provides stellar-mass profiles and mass-based structural parameters for 5557 galaxies. These have been obtained by producing the stellar-mass maps from the Hubble Space Telescope (HST) imaging data and applying the pixel-by-pixel spectral energy distribution fitting technique. The reliability of the technique has been examined in Mosleh et al. (2020) using simulated galaxies, and it has been shown that the measured parameters are robust and the sample is $\gtrsim 90\%$ complete for galaxies with $\log(M_*/M_{\odot}) \geq 9.8$ at $0.2 \leq z \leq 2$.

2.2. Stellar-mass Growth History

To select the MW progenitors, we derive the SMGHs in two different ways: (i) using the main-sequence integration (MSI) method developed by Renzini (2009) and Leitner & Kravtsov (2011) to follow SFGs on the star-forming main sequence (referred to as MW-type SMGH) and (ii) adopting the inferred SFH of MW studies (referred to as MW SMGH).

In the first approach (MW-type SMGH), the basic assumption is that present-day SFGs (including the MW) have assembled most of their stellar masses steadily and smoothly by in situ star formation. Thus, the star formation rate (SFR) of MW-type progenitors must fall within the scatter of the observed star-forming main sequence (SFR– M_* relation). The SMGH can then be iteratively calculated by obtaining the SFR

from the evolving SFR– M_* relation and taking into account stellar-mass loss. In this work, we apply the SFR– M_* relation of Speagle et al. (2014, hereafter Sp14) and that the final ($z=0$) stellar mass of the MW is $M_* = 10^{10.7} M_{\odot}$ (McMillan 2017).

In the second approach (MW SMGH), we employ the SFH estimates of MW studies to determine its SMGH directly. In this work, we use the SFH of Snaith et al. (2015, hereafter Sn15) which is obtained from fitting the solar vicinity age– $[\alpha/\text{Fe}]$ relation to a chemical evolution model. The SMGH derived by this SFH is in good agreement with the MW mass assembly history presented by Kruijssen et al. (2019).

To compare our observational results with numerical simulation, we select MW-like galaxies from the IllustrisTNG (TNG50) simulation (Nelson et al. 2019; Pillepich et al. 2019) in the following way at $z=0$ (see Park et al. 2021 for the definition of those quantities):

1. Stellar mass (<30 kpc): $M_* = 10^{10.5} - 10^{10.9} M_{\odot}$;
2. Disk-to-total ratio: $D/T > 0.5$;
3. SFR/($M_{\odot}\text{yr}^{-1}$) = [0.1, 10.0].

Figure 1 shows in panel (a) and panel (b) the SFH and SMGH of MW-type galaxies inferred from the MSI method with the SFR– M_* relation of Sp14 (red lines) of the MW galaxy from Sn15 (blue lines) and of MW-like galaxies from the TNG50 simulation (green lines). The SMGH from the MW indicates an earlier formation (consistent with Kruijssen et al. 2019) than the one from the MSI method. Figure 1(c) shows the evolution of the SFR and M_* . The large gray circle is the MW mass and SFR estimated by Licquia & Newman (2015), highlighting that our SMGHs are consistent with this estimate.

2.3. Selection of Progenitors

We select the MW progenitors at a given redshift to be all SFGs with a stellar mass consistent within ± 0.1 dex of the MW and MW-type SMGHs inferred above. SFGs are defined by their location in the rest-frame UVJ color diagram with the boundaries given in Mosleh et al. (2017). In order to reduce the uncertainties, we exclude galaxies with unreliable structural parameters (see Mosleh et al. 2020 for more details). A total of 1250 and 721 objects are identified as possible MW-type and MW progenitors up to $z \sim 1.7$ and $z \sim 2$, respectively.

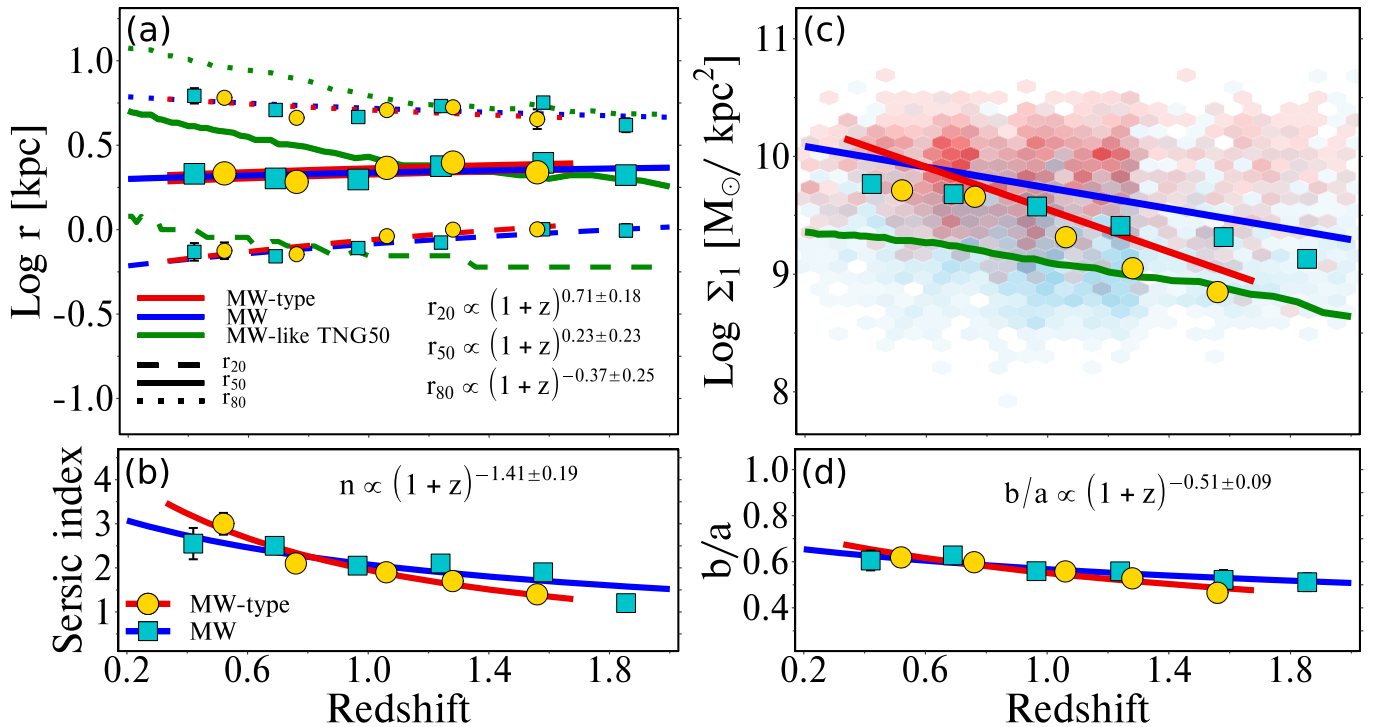


Figure 2. Evolution of the size (panel (a)), Sérsic index (panel (b)), central stellar-mass density Σ_1 (panel (c)), and axis ratio (panel (d)) with redshift for MW progenitors. The yellow circles and cyan squares are for the MW-type and MW progenitors, respectively, and the solid red and blue lines are the corresponding best fits. The green solid lines show the evolution of the radii of the TNG50 MW-like galaxies. In panel (a), dashed (small symbols), solid (large symbols), and dotted (small symbols) lines indicate the median evolution of the radii that enclose 20% (r_{20}), 50% (r_{50}), and 80% (r_{80}) of the stellar mass, respectively. In panel (c), the red and blue hex-histograms show the Σ_1 distribution of quiescent galaxies and SFGs of a stellar-mass-complete sample. A considerable decrease in r_{20} and an increase in the Sérsic index and Σ_1 are observed with cosmic time, whereas r_{50} and r_{80} remain approximately constant. In contrast, the TNG50 MW-like galaxies show a significant increase in r_{20} , r_{50} , and r_{80} with cosmic time.

In Figure 1(c), the yellow circles and cyan squares show the median of the integrated UV+IR SFRs from Whitaker et al. (2014) for the MW-type and MW progenitors, respectively. The yellow circles are different from the solid red line because the UVJ-selected SFGs do not exactly reproduce the SFR- M_* relation of Sp14. The cyan squares differ from the blue line because the UVJ-selected SFGs have typically higher SFRs than the MW at fixed stellar mass and redshift.

3. Results

3.1. Size Evolution

Figure 2(a) shows the size growth of the MW-type progenitors (yellow symbols) and the MW progenitors (cyan symbols). We focus on the stellar-mass-based radii that enclose 20% (r_{20}), 50% (r_{50}), and 80% (r_{80}) of the total stellar mass. We fit a power law of the form $r \propto (1+z)^\gamma$ to the median values to quantify the rate of size evolution.

Focusing on the evolution of MW-type galaxies (red lines and yellow circles), the half-mass sizes (r_{50}) of the progenitors remain almost constant within the redshift range of this study. The rate of r_{80} size growth is also shallow ($\gamma = -0.37 \pm 0.25$). By contrast, the r_{20} size decreases with a rate of $\gamma = 0.71 \pm 0.18$. Similar results are obtained if we focus on the MW progenitors (blue lines and cyan squares). In contrast, the sizes of MW-like galaxies from TNG50 (green lines) increase significantly with cosmic time, particularly below $z \sim 1$.

The slow rate of the half-mass size evolution for SFGs has already been alluded to by previous studies that performed the analysis at fixed masses (e.g., Suess et al. 2019a;

Mosleh et al. 2020). However, tracing progenitors makes this even more apparent. This might be caused by the simultaneous buildup of stellar mass in the core and the outskirts at large radii over time. This self-similar growth of the stellar-mass profile is consistent with a flat radial specific SFR profile, as observed at intermediate redshifts (e.g., Tacchella et al. 2015a, 2018; Nelson et al. 2016; Morselli et al. 2019).

This pattern of self-similar growth can also be seen directly in Figure 3(a), where we plot the r_{50} - M_* plane. The MW and MW-type progenitors increase their stellar mass by nearly 1 dex, while their r_{50} size remains constant ($r \propto M^\beta$ with $\beta = -0.08 \pm 0.06$). Their evolution tracks well with the r_{50} - M_* relation of Mosleh et al. (2020) for SFGs at $z = 0.3$ – 0.7 , which is not too surprising because this relation does not evolve strongly with cosmic time.

To check whether our results depend on the exact size definition (above, we have used circularized half-mass sizes) and methodology, we plot in Figure 3(b) the half-mass radius of the semimajor axis $r_{e,SMA}$ from this work and Suess et al. (2019a). Adopting $r_{e,SMA}$ instead of r_{50} leads to a weak trend in the opposite direction, i.e., $r_{e,SMA}$ weakly increases with mass and time ($\beta = 0.08 \pm 0.07$), but it is still consistent with being constant. This is expected because the axis ratio b/a increases with cosmic time for MW and MW-type progenitors (Figure 2(d)). Adopting the size measurements of Suess et al. (2019a) instead of the ones of Mosleh et al. (2020) leads to negligible changes. We conclude that our key result of negligible size growth of MW and MW-type progenitors is robust.

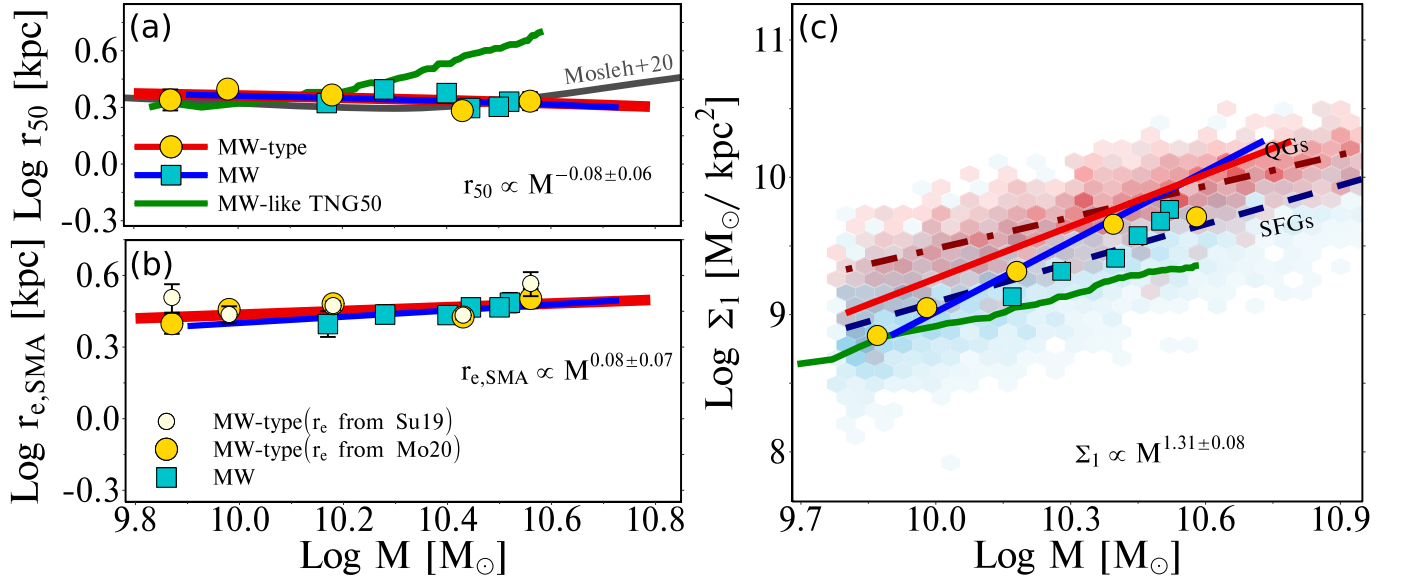


Figure 3. Evolution of the median circularized half-mass size r_{50} (panel (a)), half-mass semimajor axis size $r_{c,SMA}$ (panel (b)), and central stellar-mass density Σ_1 (panel (c)) as a function of mass. Lines and symbols are the same as in Figure 2. The gray solid line in panel (a) indicates the size–mass relation of Mosleh et al. (2020) for SFGs at $0.3 < z < 0.7$, while the dashed navy and dashed–dotted dark-red lines in panel (c) mark the Σ_1 – M_* relation for SFGs and QGs. The small beige circles in panel (b) show the size–mass evolution when adopting the size measurements of Suess et al. (2019a). MW-type progenitor galaxies exhibit a steeper evolution in the Σ_1 – M_* plane than SFGs, i.e., they have a faster central mass buildup than SFGs, consistent with the r_{20} evolution.

3.2. Growth of Central Densities

The buildup of the central density can be directly linked to an increase of the Sérsic index (n) and the stellar-mass surface density within 1 kpc (Σ_1). Panels (b) and (c) of Figure 2 show the redshift evolution of the Sérsic index n and Σ_1 for the MW-type (yellow circles) and MW progenitors (cyan squares).

We find that both the MW and MW-type progenitors increased n and Σ_1 with cosmic time, with the trend being shallower for the MW than the MW-type progenitors. For the Sérsic index n , we find $n \propto (1+z)^{-1.41 \pm 0.19}$ and $n \propto (1+z)^{-0.77 \pm 0.21}$ for the MW-type and MW progenitors, respectively. Furthermore, MW-type progenitors increase Σ_1 by nearly one order of magnitude from $z \approx 1.7$ to $z \approx 0.7$, while a shallower evolution is found at lower redshifts, independent of the parametric or nonparametric Σ_1 estimation. This is consistent with the increase in n and the decrease of r_{20} , pointing to a significant buildup of mass in the core, reaching values of Σ_1 that are consistent with quiescent galaxies (QGs). Interestingly, n reaches a value of only $n \approx 2$ by $z \approx 0.7$, compatible with a pseudo-like bulge or a thick disk rather than a classical bulge component. We caution that the results are based on a single Sérsic model. The MW-like progenitors of the TNG50 simulation (green line in Figure 2(c)) show a shallower evolution in Σ_1 – z than one of the MW-type progenitors but are roughly consistent with the MW progenitors.

The track of progenitors in the Σ_1 –mass plane is illustrated in Figure 3(c). Compared with the general relation of SFGs (dashed navy line), the MW-type and MW progenitors trace steeper relations as indicated by the red ($\Sigma_1 \propto M^{1.31 \pm 0.08}$) and blue ($\Sigma_1 \propto M^{1.71 \pm 0.19}$) lines, respectively. For comparison, the SFGs and QGs have slopes of 0.94 ± 0.01 and 0.76 ± 0.01 , respectively, in agreement with Barro et al. (2017).

Finally, for the MW-type progenitors, we tested whether the profile change is self-similar at all redshifts by comparing

the shape of their median mass profiles (Figure 4). As a comparison, we used the MW mass profile from McMillan (2017), noting that they assumed a spatially constant M_*/L . Figure 4(a) shows that the shape and slope of the profiles mostly remain the same with time, though there is some change in the central regions ($\lesssim 1.5$ kpc) at later times. The growth of stellar mass within different apertures is shown in panel (b). The MW-type progenitors grow largely self-similarly, though there is a phase of accelerated core growth between $z = 1.1$ and $z = 0.7$. At late times ($z < 0.7$), there seems to be more growth beyond 10 kpc than within.

4. Discussion and Conclusions

Our key result, which is summarized and compared with other observational (Patel et al. 2013; van Dokkum et al. 2013; Papovich et al. 2015), theoretical (Rodríguez-Puebla et al. 2017; Frankel et al. 2019), and simulated (Avila-Reese et al. 2018) studies in Figure 5, is that the progenitors of the MW galaxy grow self-similarly and have roughly a constant half-mass radius over the past 10 Gyr, while their stellar mass increases by about 1 dex. This holds while adopting two rather different SMGHs: one obtained via the MSI method (MW type; red lines) and one measured directly from the MW (MW; blue lines).

Patel et al. (2013), also using the MSI method, find a weak increase in r_{50} at the late cosmic time, while the increase in their Sérsic index is weaker and with a lower normalization than our estimate. Adopting the SFR– M_* relation of their work, we find our results still hold. We therefore attribute these differences to the increasing importance of the M_*/L gradient at late times (e.g., Mosleh et al. 2017; Suess et al. 2019b). van Dokkum et al. (2013) and Papovich et al. (2015) adopt different selection techniques to identify MW progenitors (constant comoving number density and abundance matching, and they both include QGs), which lead to shallower SMGHs than those

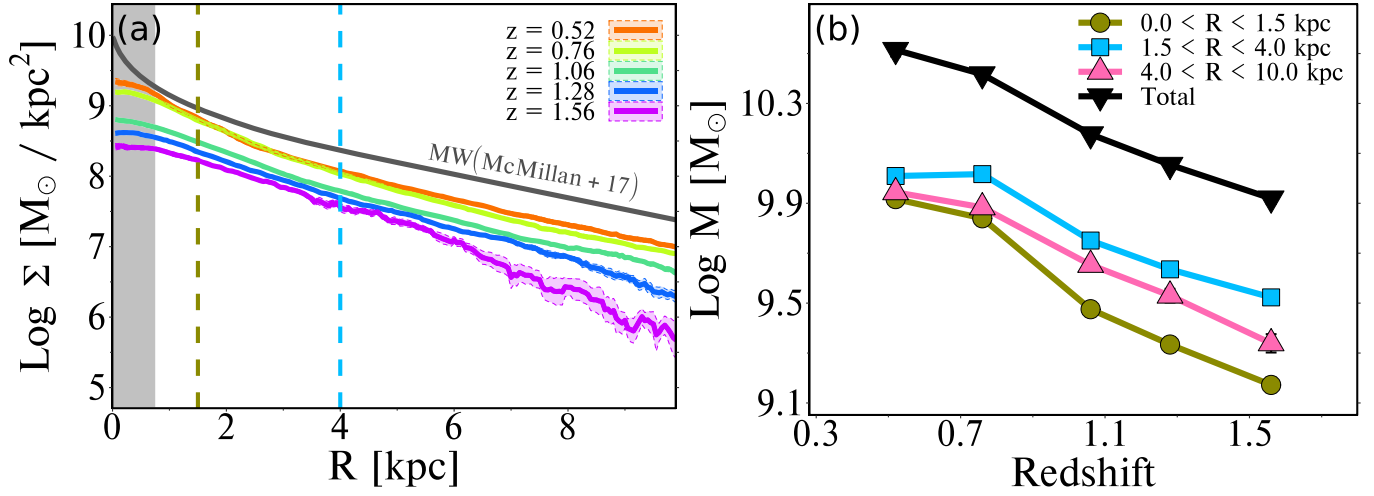


Figure 4. (a) Comparing the median stellar-mass density profiles of MW-type progenitors, along with the profiles of the MW from the best-fit parameters estimated by McMillan (2017). (b) The total stellar-mass growth within different apertures. The stellar mass in the core has more rapidly increased than that in the other regions from $z = 1.1$ to $z = 0.7$, consistent with the decrease in r_{20} and increase in Σ_1 over the same epoch (Figure 2).

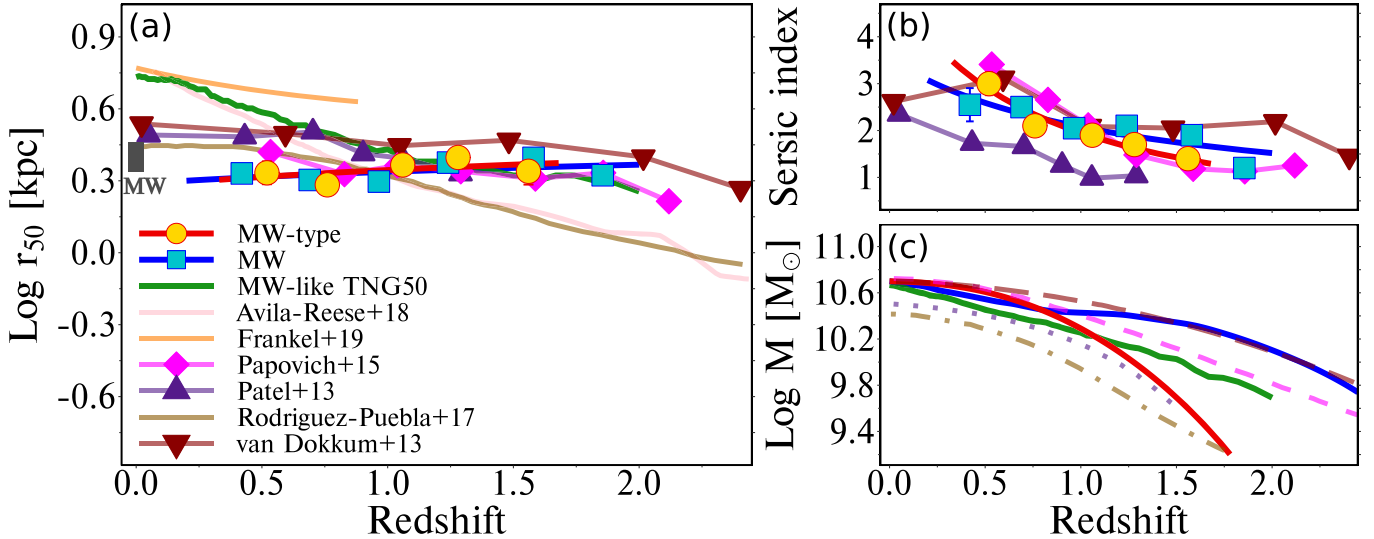


Figure 5. Comparison of the redshift evolution of r_{50} (panel (a)), Sérsic index (panel (b)), and stellar mass (panel (c)) of MW progenitors with recent observational and theoretical studies. Lines and symbols follow Figures 1 and 2. The gray rectangle represents the MW's r_{50} derived from the McMillan (2017) profile and corrected with the typical $r_{\text{mass}}/r_{\text{light}}$ from Mosleh et al. (2017). Overall, a consistent picture for the MW galaxy arises: While the stellar mass has increased by >1 order of magnitude over the past 10 Gyr, the half-mass size has roughly stayed constant. Over the same time span, the Sérsic index increased from disk like (close to 1) to 2–4 at lower redshift, consistent with the formation of a thick disk or bulge.

estimated by the MSI method (Figure 5(c)). Their inferred size growth shows a slow rate of evolution, similar to our study, despite using half-light radii. They also find that bulges have already been built by $z \sim 0.5$ (Figure 5(b)).

Rodríguez-Puebla et al. (2017) adopt a semiempirical approach for connecting galaxies to their host halos. The SMGH for the final halo mass of $10^{12}M_{\odot}$ of the MW shows a similar trend to this work (Figure 5(c)). However, the inferred size evolution, which assumes that the sizes scale as $\propto H(z)^{-0.5}$, predicts a steeper trend, particularly at $z > 1$. Moreover, Frankel et al. (2019) estimate the half-mass size evolution of the MWs low- α disk ($R = 6\text{--}13$ kpc) by fitting a global model to the ages, metallicities, and radii of APOGEE red clump stars and find a size growth of $r_{1/2} \propto (1+z)^{-0.49}$, which is in line with our r_{80} size growth, but significantly larger than our r_{50} estimates. We also find that the size evolution of MW-like galaxies in the TNG50 simulation (green line in Figure 5) is

consistent with our results at early times but shows a strong increase in more recent times ($z < 0.7$), which is contrary to our findings. This rapid increase in size is similar to that driven by Avila-Reese et al. (2018), who simulated the evolution of eight zoomed-in hydrodynamical MW-sized galaxies. As seen in Figure 5(a), r_{50} grows relatively faster than in any observational study.

A concern of our analysis is the assumption that mergers play no significant role in the buildup of the stellar mass of the MW. Kruijssen et al. (2020) and Naidu et al. (2021) estimate that the most massive mergers of the MW contributed a total stellar mass of $\log(M/M_{\odot}) \approx 10^9$, suggesting that the MW formed mainly by in situ star formation. Therefore, we conclude that mergers did not significantly affect the mass assembly of the MW progenitor, at least for the redshift range of this study.

Our analysis also has important consequences regarding the angular momentum history of galactic disks (such as the MW).

The angular momentum of a galaxy is

$$J_* \propto M_* r_{50} v_{\text{rot}}, \quad (1)$$

where v_{rot} is the rotational velocity, which increased from $z \approx 2$ to today for MW-type galaxies by a factor of ~ 1.5 (Simons et al. 2017). As discussed above, the stellar mass of the MW increased by a factor of 5–10 from $z \approx 2$ to today, while the half-mass size remains constant. Putting this all together, we find that the angular moment of MW-like disks increased over the past 10 Gyr by a factor of $J(z=0)/J(z=2) \approx 8\text{--}15$. This estimate is consistent with canonical dark matter theory (Peebles 1969; Dutton & van den Bosch 2012; Danovich et al. 2015) and not as extreme as recently claimed by Peng & Renzini (2020) and Renzini (2020), who have used observational scaling relations and inferred an increase by a factor of $\sim 20\text{--}50$. In the future, direct estimates of the angular momentum history of the MW will provide important constraints on the vorticity of the accreted gas and accretion history of satellite galaxies.

From the MW perspective, these results seem to be in accordance with the early ($z > 1$) formation of the thick disk, followed by a decrease in the SFR and a formation of a bar (Haywood et al. 2018; Bovy et al. 2019). This bar redistributed the stellar mass of the thick disk, thereby increasing the mass surface density in the core. This is consistent with our inferred increase of the Sérsic index and central stellar-mass density at $0.7 < z < 1.5$. Moreover, the mild growth of our half-mass size, in particular of $r_{e,\text{SMA}}$, is compatible with the slow thin-disk formation over the last 7–8 Gyr (Conroy et al. 2022). As shown here, connecting detailed studies of the MW galaxy with extragalactic studies of MW-like galaxies is fruitful. Upcoming telescopes (including the James Webb and the Roman Space Telescopes) will probe MW-like galaxies to higher redshifts and with better spatial resolution, allowing us to constrain the cosmic evolution of the thickness of disks and the occurrence of bars.

We thank the anonymous referee for the suggestions that helped improve the manuscript. We are also grateful to Alvio Renzini for insightful comments

ORCID iDs

Maryam Hasheminia  <https://orcid.org/0000-0003-3428-6441>
 Moein Mosleh  <https://orcid.org/0000-0002-4111-2266>
 Sandro Tacchella  <https://orcid.org/0000-0002-8224-4505>
 S. Zahra Hosseini-ShahiSavandi  <https://orcid.org/0000-0003-3449-2288>
 Minjung Park  <https://orcid.org/0000-0002-8435-9402>
 Rohan P. Naidu  <https://orcid.org/0000-0003-3997-5705>

References

- Abramson, L. E., Gladders, M. D., Dressler, A., et al. 2016, *ApJ*, 832, 7
 Avila-Reese, V., González-Samaniego, A., Colín, P., et al. 2018, *ApJ*, 854, 152
 Barro, G., Faber, S. M., Koo, D. C., et al. 2017, *ApJ*, 840, 47
 Behroozi, P. S., Marchesini, D., Wechsler, R. H., et al. 2013, *ApJL*, 777, L10
 Belokurov, V., Erkal, D., Evans, N. W., et al. 2018, *MNRAS*, 478, 611
 Bonaca, A., Conroy, C., Cargile, P. A., et al. 2020, *ApJL*, 897, L18
 Bovy, J., Leung, H. W., Hunt, J. A. S., et al. 2019, *MNRAS*, 490, 4740
 Carollo, C. M., Bschorr, T. J., Renzini, A., et al. 2013, *ApJ*, 773, 112
 Cibinel, A., Carollo, C. M., Lilly, S. J., et al. 2013, *ApJ*, 776, 72
 Conroy, C., Bonaca, A., Cargile, P., et al. 2019, *ApJ*, 883, 107
 Conroy, C., Weinberg, D. H., Naidu, R. P., et al. 2022, arXiv:2204.02989
 Danovich, M., Dekel, A., Hahn, O., et al. 2015, *MNRAS*, 449, 2087
 Dutton, A. A., & van den Bosch, F. C. 2012, *MNRAS*, 421, 608
 Frankel, N., Sanders, J., Rix, H.-W., et al. 2019, *ApJ*, 884, 99
 Gaia Collaboration, Brown, A. G. A., Vallenari, A., et al. 2018, *A&A*, 616, A1
 Haywood, M., Di Matteo, P., Lehnert, M., et al. 2018, *A&A*, 618, A78
 Helmi, A., Babusiaux, C., Koppelman, H. H., et al. 2018, *Natur*, 563, 85
 Kruijssen, J. M. D., Pfeffer, J. L., Chevance, M., et al. 2020, *MNRAS*, 498, 2472
 Kruijssen, J. M. D., Pfeffer, J. L., Reina-Campos, M., et al. 2019, *MNRAS*, 486, 3180
 Leitner, S. N., & Kravtsov, A. V. 2011, *ApJ*, 734, 48
 Licquia, T. C., & Newman, J. A. 2015, *ApJ*, 806, 96
 McMillan, P. J. 2017, *MNRAS*, 465, 76
 Miller, T. B., van Dokkum, P., Mowla, L., et al. 2019, *ApJL*, 872, L14
 Morselli, L., Popesso, P., Cibinel, A., et al. 2019, *A&A*, 626, A61
 Mosleh, M., Hosseinnejad, S., Hosseini-ShahiSavandi, S. Z., et al. 2020, *ApJ*, 905, 170
 Mosleh, M., Tacchella, S., Renzini, A., et al. 2017, *ApJ*, 837, 2
 Moster, B. P., Naab, T., & White, S. D. M. 2013, *MNRAS*, 428, 3121
 Mowla, L. A., van Dokkum, P., Brammer, G. B., et al. 2019, *ApJ*, 880, 57
 Naidu, R. P., Conroy, C., Bonaca, A., et al. 2021, *ApJ*, 923, 92
 Nelson, D., Pillepich, A., Springel, V., et al. 2019, *MNRAS*, 490, 3234
 Nelson, E. J., van Dokkum, P. G., Förster Schreiber, N. M., et al. 2016, *ApJ*, 828, 27
 Papovich, C., Labbé, I., Quadri, R., et al. 2015, *ApJ*, 803, 26
 Park, M., Tacchella, S., Nelson, E. J., et al. 2021, arXiv:2112.07679
 Patel, S. G., Fumagalli, M., Franx, M., et al. 2013, *ApJ*, 778, 115
 Peebles, P. J. E. 1969, *ApJ*, 155, 393
 Peng, Y.-j., & Renzini, A. 2020, *MNRAS*, 491, L51
 Pillepich, A., Nelson, D., Springel, V., et al. 2019, *MNRAS*, 490, 3196
 Renzini, A. 2020, *MNRAS*, 495, L42
 Renzini, A. 2009, *MNRAS*, 398, L58
 Rodríguez-Puebla, A., Primack, J. R., Avila-Reese, V., et al. 2017, *MNRAS*, 470, 651
 Simons, R. C., Kassin, S. A., Weiner, B. J., et al. 2017, *ApJ*, 843, 46
 Skelton, R. E., Whitaker, K. E., Momcheva, I. G., et al. 2014, *ApJS*, 214, 24
 Snaith, O., Haywood, M., Di Matteo, P., et al. 2015, *A&A*, 578, A87
 Speagle, J. S., Steinhardt, C. L., Capak, P. L., et al. 2014, *ApJS*, 214, 15
 Suess, K. A., Kriek, M., Price, S. H., et al. 2019a, *ApJ*, 877, 103
 Suess, K. A., Kriek, M., Price, S. H., et al. 2019b, *ApJL*, 885, L22
 Tacchella, S., Carollo, C. M., Förster Schreiber, N. M., et al. 2018, *ApJ*, 859, 56
 Tacchella, S., Carollo, C. M., Renzini, A., et al. 2015a, *Sci*, 348, 314
 Tacchella, S., Dekel, A., Carollo, C. M., et al. 2016, *MNRAS*, 457, 2790
 Tacchella, S., Lang, P., Carollo, C. M., et al. 2015b, *ApJ*, 802, 101
 Torrey, P., Wellons, S., Machado, F., et al. 2015, *MNRAS*, 454, 2770
 van der Wel, A., Franx, M., van Dokkum, P. G., et al. 2014, *ApJ*, 788, 28
 van Dokkum, P. G., Leja, J., Nelson, E. J., et al. 2013, *ApJL*, 771, L35
 Whitaker, K. E., Franx, M., Leja, J., et al. 2014, *ApJ*, 795, 104